Surface Area and Microporosity of Carbon Aerogels from Gas Adsorption and Small- and Wide-Angle X-ray Scattering Measurements

David Fairén-Jiménez,*,† Francisco Carrasco-Marín,† David Djurado,‡ Françoise Bley,§ Françoise Ehrburger-Dolle,|| and Carlos Moreno-Castilla†

Departamento de Química Inorgánica, Facultad de Ciencias, Universidad de Granada, 18071 Granada, Spain, DRFMC/SPrAM/LEMOH, UMR 5819 CEA/CNRS/UJF, CEA Grenoble, 17 rue des Martyrs, 38054 Grenoble Cedex 9, France, Laboratoire de Thermodynamique et Physico-Chimie Métallurgique, UMR 5614 CNRS-UJF-INPG, Domaine Universitaire, 38402 Saint Martin d'Hères Cedex, France, and Laboratoire de Spectrométrie Physique, UMR 5588 CNRS-UJF, Domaine Universitaire, 38402 Saint Martin d'Hères Cedex, France

Received: October 19, 2005; In Final Form: February 8, 2006

A carbon aerogel was obtained by carbonization of an organic aerogel prepared by sol−gel polymerization of resorcinol and formaldehyde in water. The carbon aerogel was then CO_2 activated at 800 °C to increase its surface area and widen its microporosity. Evolution of these parameters was followed by gas adsorption and small- and wide-angle X-ray scattering (SAXS and WAXS, respectively) with contrast variation by using dry and wet (immersion in benzene and *m*-xylene) samples. For the original carbon aerogel, the surface area, S_{SAXS}, obtained by SAXS, is larger than that obtained by gas adsorption (S_{ads}). The values become nearly the same as the degree of activation of the carbon aerogel increases. This feature is due to the widening of the narrow microporosity in the carbon aerogel as the degree of activation is increased. In addition, WAXS results show that the short-range spatial correlations into the assemblies of hydrocarbon molecules confined inside the micropores are different from those existing in the liquid phase.

1. Introduction

Carbon aerogels are novel porous carbon materials obtained by carbonization of organic aerogels. These organic aerogels can be prepared from the sol−gel polymerization reaction of organic monomers following Pekala's method.[1,2] The most widely used organic monomers are a mixture of resorcinol (R) and formaldehyde (F). Gelation is catalyzed in either basic and acid medium by using an appropriate catalyst (C).

Carbon aerogels usually have a well-developed and controlled micro- and mesoporosity and a large surface area. Carbon aerogels have a network structure of interconnected nanosized primary particles. Concerning their pore structure, micropores are related to the intraparticle structure, whereas mesopores and macropores result from the interparticle structure.[3] It is, therefore, possible to control the amount of micropores and mesopores independently, which is one of the advantages of carbon aerogels as porous carbon materials. These amounts depend on the nature and concentration of the original ingredients, the curing and drying methods of the organic aerogel, and its carbonization conditions.[4] Because the structure and texture of carbon aerogels can be designed and controlled at the nanometer scale, carbon aerogels were recently classified as nanostructured carbons.[5]

The usual method to evaluate the micropore texture and surface area of carbon materials is based on the measurements of CO_2 at 0 °C and N_2 at −196 °C. Both gases are complementary to obtain a more complete knowledge of the microporosity and the external surface of carbon materials.[6] Results obtained from gas adsorption can be supplemented with those obtained from small-angle X-ray scattering (SAXS) measurements,[7] which is not an intrusive method and can yield additional information on the surface area and microporosity of carbon materials.[8−11] Thus, gas adsorption cannot detect closed porosity, whereas SAXS detects both closed and open porosity and may, therefore, give larger apparent surface area values. Contrast variation (CV) obtained by immersion of the porous samples into a liquid allows discrimination between closed porosity and constrictions hindering the access of micropores for N_2 at −196 °C. It is also a way to obtain information about possible molecular-sieve or surface-chemistry effects.[12] Furthermore, the value of the specific surface area will be underestimated when the pore width is too narrow to accommodate one molecular layer on each wall. Conversely, this value may be overestimated when the pore width is equivalent to two to four molecular sizes.

Several authors[10,11,13−15] have combined gas adsorption and SAXS measurements to determine the surface area of organic and carbon aerogels. Results obtained showed that, depending on the synthesis method of the organic gels, micropores were or were not accessible to N_2 at −196 °C or even CO_2 at 0 °C.[10−12] In other cases,[11] the micropores were so narrow that they could not accommodate two layers of the adsorptive molecules, one on each micropore wall. Pekala et al.[14] also reported that a part of the total microporosity was not accessible to CO_2 molecules at 0 °C in high-density aerogels and in those pyrolized at temperatures above 1050 °C. According to the authors, this was due to the growth of "encapsulated" micropores similar to those present in glassy carbons. In other cases,[13,16]

* Corresponding author. Tel.: +34 958 24 32 35. Fax: +34 958 24 85 26. E-mail: fairen@ugr.es.
† Universidad de Granada.
‡ DRFMC/SPrAM/LEMOH.
§ Laboratoire de Thermodynamique et Physico-Chimie Métallurgique, Domaine Universitaire.
|| Laboratoire de Spectrométrie Physique, Domaine Universitaire.

10.1021/jp055992f CCC: $33.50
Published on Web 04/07/2006

SAXS measurements have found differences in the aerogels morphology, which leads to a different radius of gyration of the primary particles and aggregates and different shapes of aggregates.

This work was designed to study the evolution in surface area and pore texture of a carbon aerogel that was CO_2 activated at 800 °C by a combination of techniques, including physical adsorption of N_2 and CO_2 at −196 and 0 °C, respectively, and SAXS and wide-angle X-ray scattering (WAXS) with CV. This paper shows how these techniques are complementary; it gives a detailed analysis of the experimental results to avoid irrelevant interpretation. Finally, information about the presence of closed and/or narrow microporosity and its evolution during CO_2 activation as well as about the structure of solvent molecules adsorbed in pores is also discussed.

2. Experimental Section

A monolithic organic aerogel was prepared by a sol−gel polymerization reaction of R and F in water (W), following Pekala's method. The molar ratios were R/F = 0.5 and R/W = 0.08. To this mixture was added Na_2CO_3, acting as a polymerization C, with an R/C molar ratio of 800. The mixture was stirred to obtain a homogeneous solution that was cast into glass moulds (45 cm length × 0.5 cm internal diameter). The glass moulds were sealed, and the mixture was cured.[17]

After the curing cycle, the gel rods were cut into 5-mm pellets and placed in acetone (one week) to exchange water inside the pores. The gel was supercritically dried with carbon dioxide to form the corresponding monolithic organic aerogel. This sample will be referred to, in the text, as sample J-OA. Pyrolysis of sample J-OA to obtain the corresponding monolithic carbon aerogel was carried out in a 100 cm^3/min N_2 flow and by heating to 900 °C at a 1.5 °C/min heating rate and a 5 h soaking time. The sample thus obtained will be referred to in the text as J. Then two portions of this carbon aerogel were activated by heating to 800 °C in a CO_2 flow (100 cm^3/min) to obtain 14 and 35% weight losses. These samples will be referred to as J14 and J35, respectively.

Characterization of surface area, pore texture, and surface morphology was carried out by N_2 and CO_2 adsorption at −196 and 0 °C, respectively, and by SAXS and WAXS. Adsorption isotherms were measured in a conventional volumetric glass system under a 10^{-6} mbar dynamic vacuum. Prior to the adsorption measurements, samples were outgassed at 110 °C overnight under high vacuum. N_2 adsorption isotherms were analyzed by BET equation and by the α_S-method of Singh and Gregg.[18] In the latter case, the nonporous carbon used as standard was that reported by Rodriguez-Reinoso et al.[19]

The Dubinin−Radushkevich (DR) eq 1 was applied to both N_2 and CO_2 adsorption isotherms at −196 and 0 °C, respectively.

$$W = W_0 \exp\left[\left(-\frac{A}{\beta E_0}\right)^2\right] \quad (1)$$

where W is the amount absorbed at a relative pressure p/p_0; W_0 is the limiting value filling the micropores; A is the differential molar work given by $A = RT \ln P/P_0$; β is the affinity coefficient taken as 0.33 and 0.35 for N_2 and CO_2, respectively; and E_0 is the characteristic adsorption energy. The N_2 and CO_2 molar volumes were taken as 34.65 and 43.01 cm^3/mol, respectively.[6,20]

SAXS and WAXS experiments were carried out using the French CRG beamline BM2 at the European Synchrotron Radiation Facility (ESRF), Grenoble (France) and at the Laboratoire de Spectrométrie Physique, Grenoble. The SAXS and WAXS experiments were carried out with dry and wet samples. For these experiments, all carbon aerogels were ground in an agate mortar, introduced in quartz capillaries, and outgassed under high vacuum before being sealed. Wet samples were exposed to benzene or *m*-xylene vapors at relative pressure $p/p_0 = 1$. After 2 days, for equilibrium, the capillaries were filled with the respective liquid hydrocarbon and sealed.

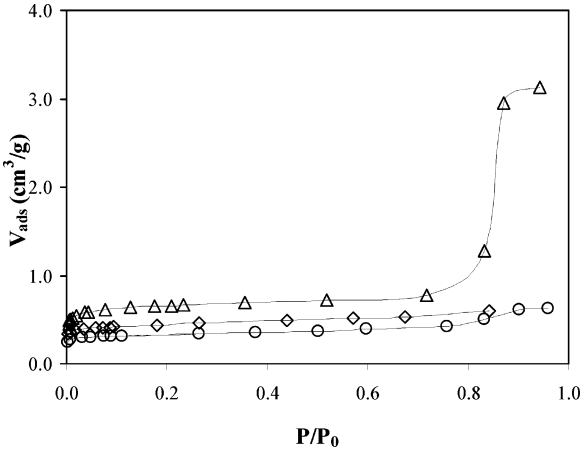

Figure 1. Nitrogen adsorption isotherms at −196 °C on carbon aerogels: ○, J; ◇, J14; △, J35.

Two distances were used to investigate scattering over a wide range of scattering vectors q, defined in eq 2

$$q = \frac{4\pi}{\lambda} \sin(\theta/2) \quad (2)$$

where λ is the wavelength and θ is the scattering angle. The incident energy was set to 12.40 keV ($\lambda = 1$ Å) and the distances were 81.4 and 212.8 cm. The beam stop was a lead disk of 1.5 mm. An indirect illumination CCD detector (Princeton Instruments) with an effective pixel size of 50 μm, cooled by a Peltier-effect device, was used. Intensity curves I(q) obtained by azimuthal averaging were corrected for grid distortion, dark current, sample transmission, and background scattering.

WAXS experiments were made using an X-ray tube (λ = 1.542 Å), a flat graphite monochromator, and a Philips PW 1835 goniometer operating in the Debye−Scherrer geometry. The total aperture of the multilinear detector (Raytech) was 16° in 2θ (800 channels). The 2θ steps were set to 0.1°, and the counting time was 45 s per step. Measurements were performed by transmission through the capillary tubes. The data were corrected from the empty glass capillary scattering and from that of the bulk solvent in the case of wet samples.

3. Results and Discussion

3.1. Adsorption Measurements. N_2 adsorption isotherms obtained on the different carbon aerogels studied are plotted in Figure 1. They are typical of microporous solids, which contain a certain meso and macroporosity development. S_{BET} values obtained from them are given in Table 1. Plots of the α_s method applied to these isotherms are depicted in Figure 2, and the corresponding micropore volume, $W_0(\alpha)$, and external surface area, S_{ext}, obtained from the above plots are collected in Table 1. S_{total} values (Table 1) are obtained from the above $W_0(\alpha)$ and S_{ext} values by converting $W_0(\alpha)$ into an apparent micropore surface area, taking into account the liquid molar volume 34.67

TABLE 1. Surface Characteristics Deduced from Adsorption and Density Measurements[a]

	J-OA	J	J14	J35
S_{BET} (m^2/g)		814	1048	1622
		α_s Method		
$W_0(\alpha)$ (cm^3/g)		0.24	0.36	0.52
S_{ext} (m^2/g)		199	220	336
S_{total} (m^2/g)		888	1220	1793
		DR Method		
N_2 W_0 (cm^3/g)		0.32	0.43	0.67
N_2 E_0 (kJ/mol)		23.7	21.9	17.5
N_2 L_0 (nm)		0.88	1.03	1.76
N_2 S_{DR} (m^2/g)		900	1210	1886
CO_2 W_0 (cm^3/g)		0.28	0.36	0.45
CO_2 E_0 (kJ/mol)		29.6	28.5	27.3
CO_2 L_0 (nm)		0.60	0.63	0.68
CO_2 S_{DR} (m^2/g)		737	947	1184
monolith density		0.35	0.33	0.26
apparent powder density, d_{app}	0.352	0.320	0.300	0.250
volume fraction of carbon, ϕ	0.176	0.160	0.150	0.125

[a] True carbon density $d_{carbon} = 2$ g/cm^3.

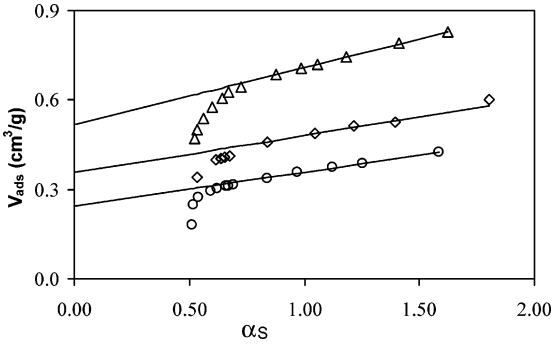

Figure 2. α_S-Plots of carbon aerogels: ○, J; ◇, J14; △, J35.

cm^3/mol and the molecular area (0.162 nm^2) of N_2 at −196 °C. This surface area is added to S_{ext}, yielding the total surface area, S_{total}.

The DR equation applied to N_2 and CO_2 adsorption isotherms on samples J and J35, as an example, is shown in Figure 3A and B, respectively. W_0 and E_0 values are obtained from these plots. The DR equation does not fit N_2 adsorption data in all relative pressure ranges (only up to about 0.05 or 0.09, depending on the sample), as can be seen in Figure 3A. So, this equation was applied in the linear portion of the plot. However, the DR equation fits very well the CO_2 adsorption data in all relative pressure ranges (Figure 3B). This is due to the big difference in saturation pressure between both adsorbates at the adsorption temperature used.

The average micropore width was estimated by means of Stoeckli and Ballerini,[21] eq 3:

$$L_0(\text{nm}) = \frac{10.8}{(E_0 - 11.4\ \text{kJ/mol})} \quad (3)$$

This equation is valid for E_0 values between 42 and 20 kJ/mol, which correspond to pore widths between 0.35 and 1.3 nm. The Dubinin eq 4 was used for smaller E_0 values[22]

$$L_0(\text{nm}) = 24/E_0\ (\text{kJ/mol}) \quad (4)$$

The W_0 values from the DR equation were also used to obtain an apparent surface area value, S_{DR}, taking into account the liquid molar volume and the molecular area of the adsorbates and assuming that W_0 was the monolayer capacity. The liquid molar volume and molecular area of CO_2 at 0 °C was taken as

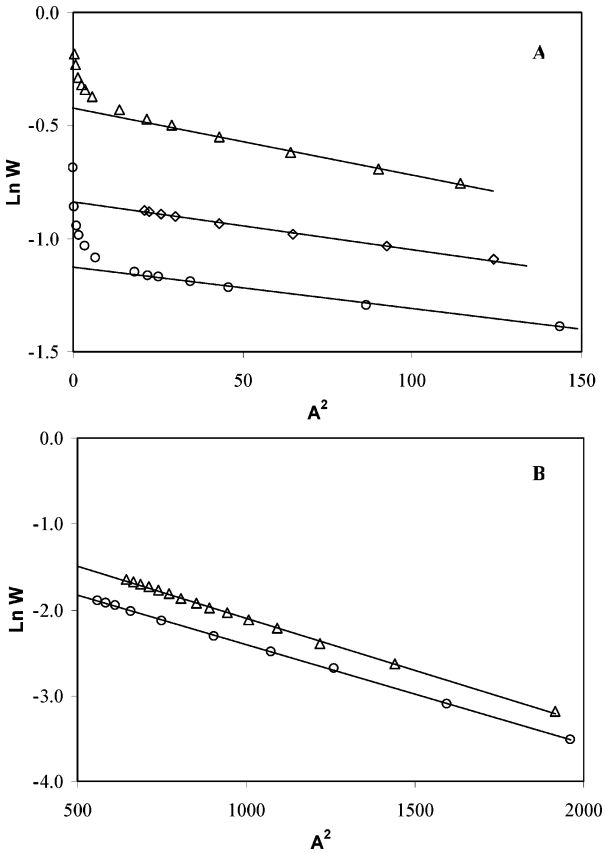

Figure 3. DR equation applied to N_2 (A) and CO_2 (B) adsorption isotherms at −196 and 0 °C, respectively, on carbon aerogels: ○, J; ◇, J14; △, J35.

42.72 cm^3/mol and 0.187 nm^2, respectively. All of these values are given in Table 1.

Although the BET model is not suitable to describe the adsorption of N_2 at −196 °C on microporous carbons, it is widely used to obtain an apparent surface area, S_{BET}. Nevertheless, the limitations of this approach should be kept in mind.[6] S_{BET}, $W_0(\alpha)$, and the external surface area of the carbon aerogels increase with their degree of activation.

S_{BET}, S_{total}, and S_{DR} increase with the degree of activation, but S_{BET} remains systematically smaller than S_{total}. This feature has been pointed out by other authors.[20,23,24] It is a consequence of the limitations of the BET model. However, S_{total} and S_{DR} from N_2 adsorption are quite similar. Table 1 also shows that around 20% of the total surface area of samples corresponds to external surface area contained in meso and macropores.

A more-detailed characterization of the microporosity is given in Table 1. It is well-known[6,25] that the micropore volume obtained from CO_2 adsorption at 0 °C yields the volume of narrow micropores (below about 0.7 nm width), whereas the total micropore volume is obtained from N_2 adsorption at −196 °C if there are no pore constrictions at their entrance. The value of $W_0(N_2)$ is slightly higher than $W_0(CO_2)$ in sample J, indicating a certain homogeneity in the micropore size distribution. For the activated carbon aerogels, $W_0(N_2)$ is always larger than $W_0(CO_2)$. The difference increases with the degree of activation in parallel with an increase in the average micropore width. This variation indicates that narrow micropores are widened during activation, resulting in a more heterogeneous microporosity. Differences found with W_0 values determined from N_2 and CO_2 adsorption isotherms also explain the differences of the apparent surface areas obtained from W_0 values

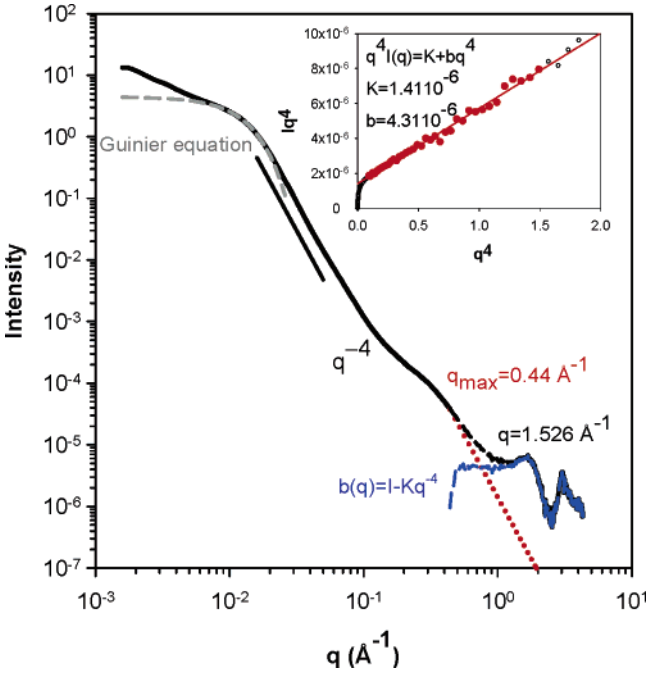

Figure 4. Intensity versus q for dry sample J (continuous line). Long dashed line refers to the Guinier equation, and the dotted line refers to the Porod's law.

3.2. SAXS/WAXS Investigation of the Dry Samples. Figure 4 shows the variation of the intensity I scattered by sample J as a function of q. In the low-q domain, the curve can be fitted by a Guinier equation:

$$I(q) = I_0 \exp\left[-\frac{(qR_G)^2}{3}\right] \tag{5}$$

yielding the radius of gyration R_G of the aerogel particles. Considering the simplest assumption of nearly spherical particles, thus, their diameter d_c can be deduced from R_G by eq 6:

$$d_c = 2R_G\sqrt{5/3} \tag{6}$$

The values of R_G and d_c are equal to 12.8 and 33 nm, respectively (Table 2). The intensity uptake at lower q results from the fact that, in aerogels, these particles are arranged in a network. Above about 2×10^{-2} Å^{-1}, the intensity scales as q^{-4} (Porod's law) as a result of the scattering of the external surface of these particles. A deviation of the Porod's law is observed above about 5×10^{-2} Å^{-1}. This feature stems from inter- and intraparticle disorder, that is, meso and micropores. The shoulder observed above 0.1 Å^{-1} is characteristic of microporosity. At higher q values, in the WAXS domain, the curve displays two broad Bragg peaks (S1 and S2), located for this sample at 1.67 and 3.03 Å^{-1}, corresponding to spacings equal to $L = 2\pi/q = 3.76$ and 2.07 Å, respectively. These peaks may result from spatial correlation between elementary diffusing carbon objects (inter-objects correlation) and carbon atoms (intra-object correlation), respectively. As expected, these distances are higher than the L_c and L_a values of graphite (3.35 and 1.42 Å, respectively). There are at least two reasons for explaining this result. First, these aerogels are known to be nongraphitizable carbons and, second, due to the amorphous character of the material, the nearest approach distance between objects which can be deduced from these measurements would be divided by a factor of 1.22, according to the reference.[26] As is also shown elsewhere,[10] the first Bragg peak displays a tail toward the low-q region stemming from the larger out-of-plane spacing (>7 Å) responsible for the microporosity (P1).

When calibration of the intensity by means of a standard cannot be made accurately, as in the case of powder samples, a determination of the surface area is generally achieved by using the method of the invariant, eq 7

$$Q = \int_0^\infty I(q)q^2\,dq \tag{7}$$

yielding the extend S_v of the carbon−air interface by unit volume of sample (in m^2/cm^3)

$$S_v = \frac{A}{V} = 10^4\pi\phi(1-\phi)\frac{K}{Q} \tag{8}$$

where ϕ is the volume fraction of carbon and K is the prefactor in the Porod's law describing scattering coming from the final surface:

$$K = \lim_{q\to\infty}\{I(q)q^4\} \tag{9}$$

The specific surface area S_{SAXS} (expressed in m^2 per gram of sample) is obtained by

$$S_{SAXS} = 10^4\pi\phi(1-\phi)\frac{K}{Qd_{app}} \tag{10}$$

Because the samples are microporous, the Porod's law domain is crossing over the scattering region resulting from the internal structure (interplane correlation). As a first approximation, it may be assumed that this signal $b(q)$ is constant and equal to b.[9−11] The total intensity would be then $I(q) = Kq^{-4} + b$; hence, $I(q)q^4 = K + bq^4$. The inset in Figure 4 shows that this equation is actually verified and gives the values of K and b. It follows that eq 7 becomes:

$$Q = \int_0^\infty (I(q) - b)q^2\,dq \tag{7a}$$

which will be used in eqs 8 and 10. The value of Q is sensitive to both the upper and the lower limits of eq 7a. The contribution from the upper limit is determined by using eq 11.

$$\int_{q_{max}}^\infty (I(q) - b)q^2\,dq = \int_{q_{max}}^\infty \frac{K}{q^2}dq = \frac{K}{q_{max}} \tag{11}$$

where q_{max} is the value of q above which the contribution of the carbon structure can no longer be neglected. The lower limit could be actually $q = 0$ if one assumes that the Guinier equation describes the $I(q)$ when $q \to 0$. We have verified that the difference between the values of Q obtained by this method and the values of Q obtained by the integration of the experimental data above the lower limit, $q_{min} = 1.5 \times 10^{-3}$ Å^{-1}, amounts to less than 1%. Thus, the value of Q is obtained as follows:

$$Q = \Delta q\sum_{q_{min}}^{q_{max}}(I(q) - b)q^2 + K/q_{max} \tag{12}$$

For sample J, one gets $S_{SAXS} = 1300$ m^2/g. Uncertainty estimated by taking into account all the possible errors, particularly on scattered intensity and volume fraction, is close to ±130 m^2/g (i.e., 10%).

Q can also be used as a normalization factor for the SAXS curves, making possible a precise comparison of the different

TABLE 2. Information Obtained by SAXS/WAXS and a Comparison with That Obtained by Gas Adsorption

	J-OA	J	J14	J35
R_G (nm)	15.1 ± 0.5	12.8 ± 0.5	12.7 ± 0.5	12.5 ± 0.5
particle diameter $d_s = 2R_G\sqrt{5/3}$	38.9 ± 0.5	33.0 ± 0.5	32.8 ± 0.5	32.2 ± 0.5
Q	8.7×10^{-6}	13.7×10^{-6}	16.9×10^{-6}	12.8×10^{-6}
$10^4 \pi K/Q$	660	3204	3833	4367
b/Q	0.45	0.31	0.34	0.13
q_{max} (Å^{-1})	0.227	0.426	0.468	0.497
$\phi(1-\phi)$	0.14	0.13	0.12	0.11
S_v (m^2/cm^3)	92.4	416	460	480
S_{SAXS} (m^2/g)	264 ± 25	1300 ± 130	1533 ± 150	1921 ± 190
S_{SAXS}/S_{BET}		1.6	1.5	1.2
S_{SAXS}/S_{total}		1.5	1.3	1.1

samples investigated (Figure 5). This figure shows the major differences between organic and carbonized aerogel:

(i) The appearance of a shoulder in the carbon aerogel that does not exist in the organic precursor, characteristic of the formation of micropores inside the aerogel particles, as already mentioned above; this feature is quantified by the large difference in the surface area (S_{SAXS} = 264 m^2/g for the organic aerogel and 1300 m^2/g for the carbonized one.

(ii) The shrinkage of the carbonized samples as shown by the decrease of the particle diameter (Table 2) from nearly 39 nm for J-OA to 33 nm for J.

(iii) As expected, the short scale structure is different in the polymer and in the carbon material.

(iv) Interestingly, an isoscattering point can be seen near 0.15 Å^{-1}; a similar feature occurring at 0.045 Å^{-1} was reported and discussed by Calo and Hall[8] in the case of the activation of saran char.

The activation of sample J seems to have an effect on the large-scale structure, which is difficult to interpret without the support of electron microscopy images. The slight decrease of the particle diameter with increasing burnoff is probably not significant. For J35, the relative contribution of the intensity of P1 and S1 clearly changes (Figure 6). The most visible effect of activation is, as expected, the increase of the SAXS surface area (Table 2) as it is for the surface area determined by adsorption.

The most remarkable fact coming out from the series of adsorption and SAXS measurements is the large difference between the surface area determined by gas adsorption and the surface area determined by SAXS for the nonactivated sample (J), which tends to vanish after 35% burnoff. There are several possible explanations: constrictions yielding diffusional hindrance for nitrogen molecules at −196 °C, closed porosity, or micropores that are too narrow to accommodate one molecular layer on each wall.[11] The existence of constrictions can probably be discarded because the adsorption of CO_2 yields micropore volumes (or surface areas) that are slightly smaller but not larger than the adsorption of N_2 at low temperature (Table 1). DR analysis of the CO_2 adsorption isotherms reveals the presence of narrow micropores. This feature could be in favor of the third explanation, but it was necessary to check the second possible explanation: closed microporosity. To this end, the method of CV was used. A discussion about the surface areas will be continued afterward.

3.3. SAXS/WAXS CV and Adsorbate Structure Measurements. Figure 7 shows the scattering curve obtained for sample J immersed in benzene. The curve is located below that of the dry J sample as a result of the contrast modification: carbon−air for the dry sample and carbon−benzene for the wet sample. The electronic density of a given medium is

$$\rho_e = N_A r_e d \sum_i N_i Z_i / \sum_i N_i M_i \qquad (13)$$

(where N_A is the Avogadro number, r_e the electron radius, d

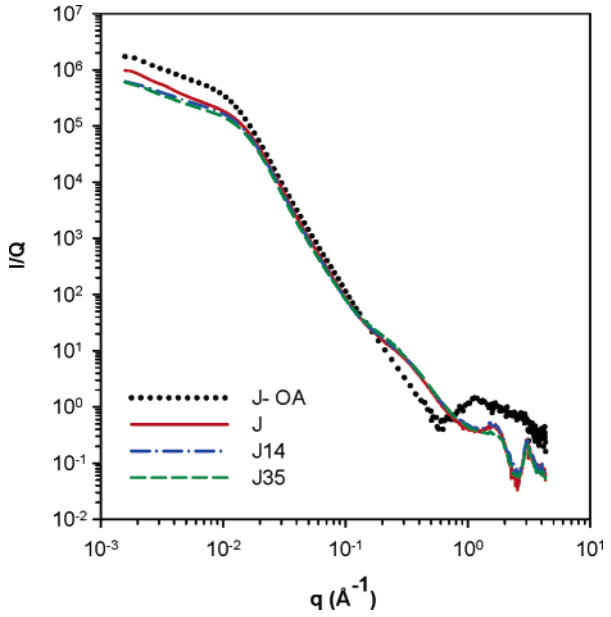

Figure 5. SAXS−WAXS curves for dry samples J-OA, J, J14, and J35.

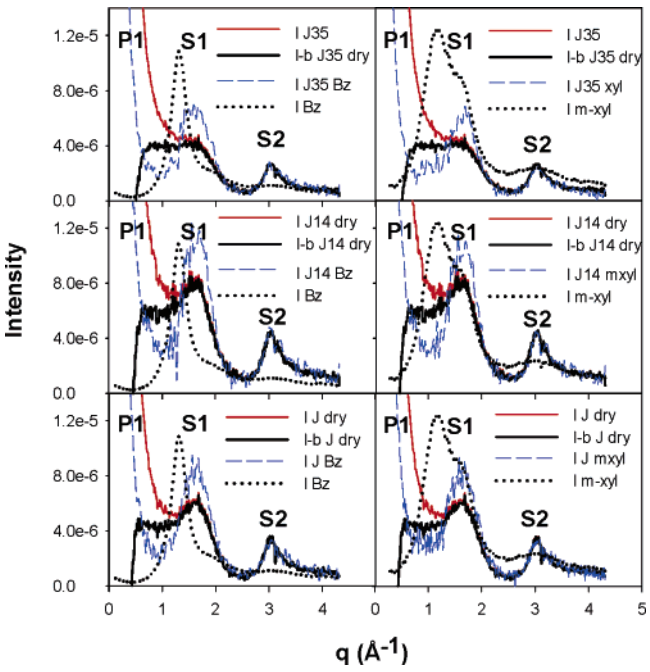

Figure 6. WAXS intensity versus q curves for samples J, J14, and J35. Comparison between dry and wet samples.

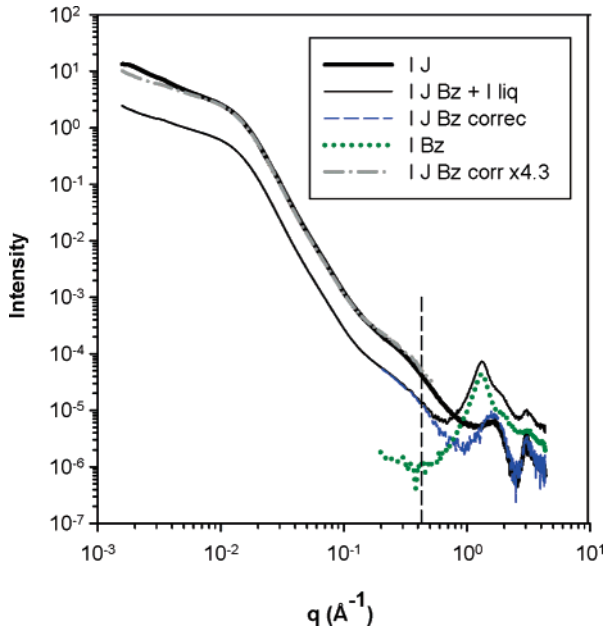

Figure 7. SAXS−WAXS curves for dry J and wet with benzene J, with and without corrections.

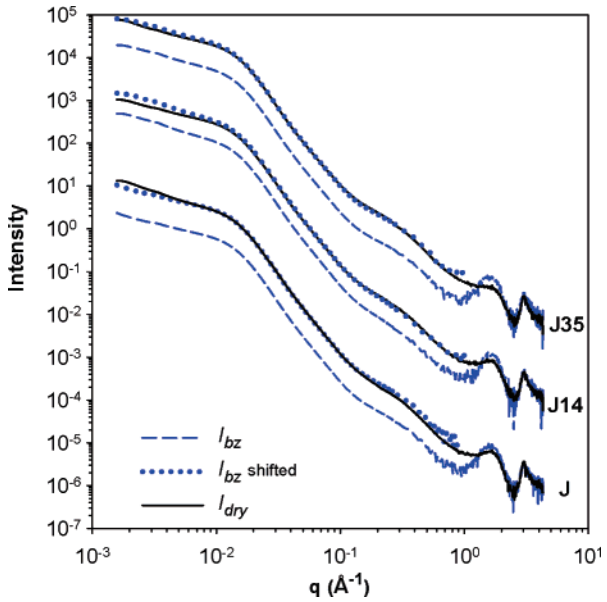

Figure 8. Intensity versus q curves for samples J, J14, and J35. Dry (continuous line), wet with benzene (long dashed line), and shifted wet with benzene (dotted line).

the density, and Z and M, the atomic number and mass, respectively). It follows that the ratio

$$C_e = I_{wet}(q)/I_{dry}(q) = (\rho_{eC} - \rho_{eBz})^2/(\rho_{eC})^2 \qquad (14)$$

between the intensity scattered by the wet sample, $I_{wet}(q)$, and the dry sample, $I_{dry}(q)$, is equal to 0.28 with $d_{carbon} = 2$ g/cm^3 and using the value of the liquid density for benzene (the same value is obtained for *m*-xylene). The dash−dotted curve plotted in Figure 7, overlapping $I_{dry}(q)$ in the middle of the q domain, corresponds to a shift F_{exp} equal to 4.2, that is, $C_{exp} = 0.24$, which is larger than the expected C_e. This difference results from the fact that the compactness of the powder immersed in the liquid in the capillary tube is not homogeneous and could be different from that of the dry sample. Furthermore, as it will be explained below, an accurate normalization of $I_{wet}(q)$ by Q is not possible.

The extra intensity shown in the high-q domain in curve $I_{C+Bz}(q)$ results from the scattering of benzene $I_{benzene}(q)$ (dotted curve), which has to be subtracted. Because the exact amount of benzene $fI_{benzene}(q)$ to be subtracted is not known precisely, the following procedure was used: the values of f are adjusted to make the second Bragg peaks (3.03 Å^{-1}) overlapping. The curve $I_{wet}(q) = I_{Bz}(q) = I_{C+Bz}(q) - fI_{benzene}(q)$ (thin dashed lines in Figure 7) indicates that, in these conditions, the first Bragg peaks coming from the interplane correlation in carbon do not match. In other words, the shape of the curve $I_{benzene}(q)$ measured for bulk liquid benzene, which was subtracted from $I_{C+Bz}(q)$ is different from that resulting from the scattering of benzene confined in micropores (or, at least, part of it, because there is an excess of liquid in these samples), which should be subtracted to get the same peak as for $I_{dry}(q)$. It follows that the structure of confined benzene must be different from that of the bulk liquid. Figure 6 shows that the same effect is observed also for *m*-xylene for all three samples (J, J14, J35). Such results, expected from molecular simulations[27,28] agree with those obtained for other molecules.[29] This feature has also two very important consequences. The first one is that the density of molecular assemblies adsorbed in micropores is different from that of bulk liquid, as already discussed by several authors[28] but generally ignored. Thus, the micropore volume deduced from adsorption measurements by assuming the validity of the Gurvitch rule can be considered only as a first approximation. The second consequence concerns the value of b used to determine K, Q, and, therefore, the surface area. The decrease of $b = b_{wet}$ in the wet sample is expected because b_{wet} stems from the largest out-of-plane spacing (i.e., micropores filled by adsorbate up to a given extent). Meanwhile, b_{wet} also results from the subtraction of $fI_{benzene}(q)$, which is incorrect. As a result, it is not possible to determine unambiguously the value of K, Q, and, therefore, the surface area in different solvents. Such a determination would require the calculation of the scattering curve of confined benzene and an investigation of systems prepared by vapor adsorption at saturation pressure, without excess of liquid.

We remind that our goal is to investigate the accessibility of the adsorbate to the microporosity, that is, to check for closed microporosity. To this end, we will compare the shape of the curves $I_{dry}(q)$ and $I_{wet}(q)$. Because of the uncertainty on the value of Q for the wet samples, discussed above, the curves are not normalized by Q. The curves obtained for samples J, J14, and J35 dry and immersed in benzene are compared in Figure 8. The dotted lines correspond to $I_{bz}(q)$, which has been shifted to overlap $I_{dry}(q)$ in the intermediate q domain (0.03−0.06 Å^{-1}). It appears that these curves overlap quite well, except in the low-q domain and in the high-q domain for sample J. For a more precise comparison, the ratio $C_{exp} = I_{wet}/I_{dry}$ was calculated for benzene and *m*-xylene for all samples (Figure 9). Because the value of C_{exp} cannot be determined precisely, the curves were arbitrarily shifted and plotted on a logarithmic scale. The aim is to compare the shape of these curves without introducing any further hypothesis. As shown in Figure 7, the contribution to the total scattering of the internal structure of both carbon and benzene or *m*-xylene can be neglected below q_{max}. In this domain, C_{exp} (eq 14) will remain constant if one assumes that the density of carbon and that of the adsorbate is constant. The decrease of the adsorbate density down to zero if the whole micropore surface is not covered (as for closed porosity) yields an increase of C_{exp}, and an increase of the adsorbate density leads to a decrease of C_{exp}. The curves corresponding to the variation of C_{exp} versus q are plotted in Figure 9. For sample J,

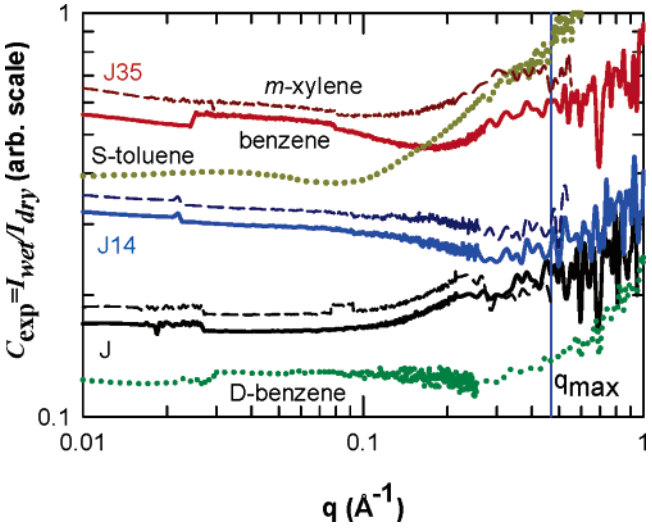

Figure 9. CV in benzene (continuous line) and *m*-xylene (long dashed line) samples for J, J14, and J35. Samples S (with toluene) and D (with benzene) are also included. *Crenels* are artifacts due to slight problems of overlapping in the region where the curves coming from the different geometries are combined.

C_{exp} remains nearly constant up to about 0.1 Å^{-1} for both adsorbates. Above this value, C_{exp} starts to increase slowly. On the same figure are also plotted the curves obtained for two other nonactivated aerogels investigated earlier:[11]

(1) Sample D, immersed in benzene, for which C_{exp} remains nearly constant up to q_{max}, indicating the absence of closed porosity.

(2) Sample S, immersed in toluene, characterized by a strong increase of C_{exp}, which suggests the existence of closed porosity.

A comparison between this series of samples suggests that the microporosity of sample J is not completely accessible to benzene or *m*-xylene. After activation (sample J14), the curves are slowly decreasing up to above q_{max}. This feature suggests (i) that the density of the adsorbates increases with q, that is, when the size of the micropores probed decreases and (ii) that there is no closed porosity anymore. For sample J35, for which gas adsorption measurements (Figure 2 and Table 1) indicate a wide distribution of pore sizes, the shape of the curves could be related also to fluctuations of density as a function of pore size.[27,28]

Finally, carbon aerogel J contains probably, before activation, some closed porosity that disappears after activation in sample J14. For sample J, S_{SAXS} is significantly larger than S_{BET} or S_{total} ($S_{SAXS}/S_{BET} = 1.6$, Table 2). The difference stems partly from the existence of some closed microporosity and partly from the fact that the micropores are too narrow to accommodate one N_2 layer on each wall. For sample D, yet showing no closed microporosity, S_{SAXS}/S_{BET} is larger ($S_{SAXS}/S_{BET} = 2$),[11] but the micropore size ($L_{CO_2} = 0.59$ nm and $L_{N_2} = 0.62$ nm), determined by means of eq 3, is slightly smaller than that of sample J ($L_{CO_2} = 0.60$ nm and $L_{N_2} = 0.88$ nm, Table 1). Although there is no closed microporosity for sample J14, S_{SAXS}/S_{BET} remains significantly larger than 1 ($S_{SAXS}/S_{BET} = 1.5$). Thus, as for sample D, the difference between S_{SAXS} and S_{BET} results from the fact that the average size of the micropores is still not large enough in J14 ($L_{CO_2} = 0.63$ nm and $L_{N_2} = 1.03$ nm). After 35% activation (sample J35), the size of the micropores increases ($L_{CO_2} = 0.68$ nm), and the ratio S_{SAXS}/S_{BET} decreases accordingly. In fact, the ratio S_{SAXS}/S_{DR} is very close to 1. This observation strengthens our assumption, which was to explain the difference between the surface area obtained by SAXS and the surface area obtained by gas adsorption, in absence of closed microporosity, by the impossibility to cover each wall of narrow micropores by an adsorbed monolayer. In other words, in such a situation, gas adsorption techniques underestimate the geometrical extension of the carbon−air interface accessible to small molecules.

4. Conclusion

SAXS and WAXS combined with CV techniques, on one hand, and gas adsorption techniques, on the other hand, are complementary methods for investigating microporous solids. Gas adsorption provides information about the *real* number of molecules that can be adsorbed by a given microporous solid that is essential for any application but may fail in transforming this information into a geometric estimation of the extension of the carbon surface; the reason for that is that the size of the probe (molecules) is larger or of the same order of magnitude as the surface roughness.

SAXS/WAXS provides information about the geometric extent of the carbon−air interface, accessible or not to molecules; a comparison with the surface area obtained by gas adsorption will give more precise information about the texture of the microporous solid in relation with the method of preparation and allow a decision about the need for activation. WAXS measurements are necessary to get a precise determination of the Porod's domain, particularly the value of b.

A comparison between scattering curves obtained for the dry sample and scattering curves obtained for the sample immersed in a liquid (CV) allows a decision about whether the difference between SAXS and adsorption surface area originates from the micropore size effect in adsorption, from closed porosity, or both. WAXS measurements of dry and wet samples are essential (i) for a precise subtraction of the adsorbate scattering and (ii) for checking if the structure of the bulk liquid which was subtracted is the same as that of the adsorbate. If not, the value of b used to determine the Porod's factor K, the invariant Q and, therefore, a surface area of the wet sample, and the contrast, C_{exp}, is incorrect because it contains terms coming from the adsorbate structure. Accordingly, the adsorbate structure can be deduced by using our methodology, providing that only micropores are filled (no excess of bulk liquid). It follows also that ignoring the effect of the micropore size on the adsorbate structure and, therefore, the adsorbate density may yield an irrelevant interpretation of the experimental results. Therefore, without a model of the adsorbate structure, the variation of C_{exp} with q for q larger than about 0.4 Å^{-1} may become meaningless. Nevertheless, we have shown that the analysis of the shape of $C_{exp}(q)$ below this limit allows a qualitative characterization of the carbon aerogel that shows the role of the polymer-synthesis conditions. This methodology was used for a series of carbon aerogels that have been prepared in different well-defined conditions. The results will be discussed in a future paper.

Acknowledgment. The University of Granada group acknowledges financial support from MCYT, MEC, and FEDER, projects MAT2001-2874 and CTQ2004-03991. We are grateful to the ESRF, Grenoble, for access to the French CRG beamline D2AM and the help of its technical staff, J. F. Berar, N. Boudet, B. Caillot, and S. Arnaud.

References and Notes

(1) Pekala, R. W. *J. Mater. Sci.* **1989**, *24*, 3221−3229.
(2) Pekala, R. W. U.S. Patent 4,873,218, 1989.
(3) Yoshizawa, N.; Hatori, H.; Soneda, Y.; Hanzawa, Y.; Kaneko K.; Dresselhaus, M. S. *J. Non-Cryst. Solids* **2003**, *330*, 99−105.

(4) Al-Muhtaseb, S. A.; Ritter, J. A. *Adv. Mater.* **2003**, *15*, 101−114.
(5) Inagaki, M.; Kaneko, K.; Nishizawa, T. *Carbon* **2004**, *42*, 1401−1417.
(6) Rodríguez-Reinoso, F.; Linares-Solano, A. In *Chemistry and Physics of Carbon*; Thrower, P. A., Ed.; Marcel Dekker: New York, 1989; Vol. 21, p 11.
(7) Porod, G. In *Small-Angle X-ray scattering*; Glatter, O., Kratky, O., Eds.; Academic Press: London, 1982.
(8) Calo, J. M.; Hall, P. J. *Carbon* **2004**, *42*, 1299−1304.
(9) László, K.; Marthi, K.; Rochas, C.; Ehrburger-Dolle, F.; Livet, F.; Geissler, E. *Langmuir* **2004**, *20*, 1321−1328.
(10) Berthon-Fabry, S.; Langohr, D.; Achard, P.; Charrier, D.; Djurado, D.; Ehrburger-Dolle, F. *J. Non-Cryst. Solids* **2004**, *350*, 136−144.
(11) Ehrburger-Dolle, F.; Fairén-Jiménez, D.; Berthon-Fabry, S.; Achard, P.; Bley, F.; Carrasco-Marín, F.; Djurado, D.; Moreno-Castilla, C.; Morfin, I. *Carbon* **2005**, *43*, 3009−3012.
(12) Hua, D. W.; D'Souza, J. V.; Schmidt, P. W.; Smith, D. M. In *Characterization of Porous Solids III*; Rouquerol, J., Rodríguez-Reinoso, F., Sing, K. S. W., Unger, K. K., Eds.; Elsevier: New York, 1994; pp 255−261.
(13) Barbieri, O.; Ehrburger-Dolle, F.; Rieker, T. P.; Pajonk, G. M.; Pinto, N.; Rao, V. *J. Non-Cryst. Solids* **2001**, *285*, 109−115.
(14) Reichenauer, G.; Emmerling, A.; Fricke, J.; Pekala, R. W. *J. Non-Cryst. Solids* **1998**, *225*, 210−214.
(15) Brand, R.; Fricke, J. *J. Non-Cryst. Solids.* **2004**, *350*, 131−135.
(16) Horikawa, T.; Hayashi, J.; Muroyama, K. *Carbon* **2004**, *42*, 1625−1633.
(17) Moreno-Castilla, C.; Maldonado-Hódar, F. J. *Carbon* **2005**, *43*, 455−465.
(18) Gregg, S. J.; Singh, K. S. W. In *Adsorption, surface area and porosity*; Academic Press: London, 1982.
(19) Rodríguez-Reinoso, F.; Martín-Martínez, J. M.; Prado-Burguete, C.; McEnaney, B. *J. Phys. Chem.* **1987**, *91*, 515−516.
(20) Stoeckli, F.; Centeno, T. A. *Carbon* **2005**, *43*, 1184−1190.
(21) Stoeckli, F.; Ballerini, L. *Fuel* **1991**, *70*, 557−559.
(22) Dubinin, M. M. *Carbon* **1985**, *23*, 373−380.
(23) Kaneko, K.; Ishii, C.; Ruike, M.; Kuwabara, H. *Carbon* **1992**, *30*, 1075−1088.
(24) Setoyama, N.; Suzuki, T.; Kaneko, K. *Carbon* **1998**, *36*, 1459−1467.
(25) Cazorla-Amorós, D.; Alcañiz-Monge, J.; de la Casa-Lillo, M. A.; Linares-Solano, A. *Langmuir* **1998**, *14*, 4589−4596.
(26) Guinier, A. In *Diffraction in Crystals, Imperfect Crystals and Amorphous Bodies*; Dover Publications, Inc.: New York, 1994; Chapter 3, pp 72−73.
(27) Lastoskie, C.; Gubbins, K. E.; Quirke, N. *J. Phys. Chem.* **1993**, *97*, 4786−4796.
(28) Biggs, M. J.; Buts, A.; Williamson, D. *Langmuir* **2004**, *20*, 5786−5800.
(29) Ohkubo, T.; Kaneko, K. *Colloids Surf., A* **2001**, *187−188*, 177−185.